University of Toronto
Division of Engineering Science

Final Design Review Report

AER406 Aircraft Design
Team 2

Alexander Hong
(997584706)
Sebastian Kai van Es
(997467076)
Pankaj Saini
(997581344)

March 21, 2014

Executive Summary

This report details the final design for Group 2's conventional aircraft. Engineering drawings, control surface dimensions, and a full mass breakdown of the the aircraft are presented. A construction plan is also presented, which includes the approach we will be using to build the aircraft. Thorough performance, structural, and stability analysis to prove our design are also included in this document. The aircraft is designed to carry at least 1000 cargo units with a predicted flight speed of 16.75 m/s. The design aims to score a total of 1000 points or higher.

Revision History

Version	Changes	Author
1.0	Initial document creation	Group 2
1.1	Performance Analysis Added	Kai van Es
1.2	CAD model update	Pankaj Saini
1.3	Structural Analysis Update	Alex Hong
1.4	Final Revision	Group 2

Contents

Acronyms **6**

1 Overview **7**
1.1 Design Objectives . . . 7
1.2 Cargo Configuration . . . 7
1.3 Propeller Selection . . . 7
1.4 Profile Selection . . . 8

2 Detailed Design **9**
2.1 Fuselage . . . 9
2.1.1 Main Fuselage . . . 9
2.1.2 Tail Fuselage . . . 10
2.1.3 Cargo Placement . . . 11
2.1.4 Engine Mount . . . 11
2.1.5 Wing Attachment . . . 12
2.2 Wing . . . 12
2.2.1 Main Spar . . . 12
2.2.2 Ribs . . . 12
2.2.3 Rear Spar . . . 13
2.2.4 Servo Mount . . . 14
2.2.5 Sheeting . . . 14
2.3 Tail . . . 15
2.4 Mass Budget . . . 16

3 Performance Analysis **17**
3.1 Level Flight . . . 17
3.2 Turn . . . 18
3.3 Structural Analysis . . . 19
3.3.1 Main Spar . . . 19
3.3.2 Tail . . . 20
3.4 Stability . . . 22
3.4.1 Static Stability . . . 22
3.4.2 Trim Deflections and Hinge Moments . . . 22
3.4.3 Dynamic Stability . . . 23
3.5 Take-off . . . 23

4 Flight Score Prediction **25**

5 Future Work **26**

A Static Derivatives **27**

B Calculations **28**
B.1 Structural Analysis . . . 28

List of Figures

1 Fuselage Main Section . . . 9
2 Main Section Bulkheads . . . 10
3 Fuselage Tail Section . . . 10
4 Cargo Layout and Hatches . . . 11
5 Engine Attachment . . . 11
6 Example of Wing-Fuselage Attachment . . . 12
7 Main Spar . . . 13
8 Rib Cross Section - Aileron . . . 13
9 Rear Spar . . . 13
10 Wing Servo Mount . . . 14
11 Wing Sheeting . . . 14
12 Tail . . . 15
13 Tail Fuselage Mounting . . . 15
14 Thrust Required and Thrust Available . . . 17
15 Progession of a Turn . . . 18
16 Acceleration After a Turn . . . 19
17 Stress analysis on main spar loading . . . 20
18 Stress analysis on tail loading . . . 20
19 Stress analysis on cargo loading . . . 21
20 Takeoff Distance vs Headwind . . . 24
21 Flight Score vs Headwind . . . 25
22 Finite Element Analysis on Fuselage . . . 28
23 Finite element analysis of tail . . . 29
24 Finite element analysis of main spar . . . 30

List of Tables

1 Mass Budget 16
2 Drag Coefficient Breakdown 17
3 Static Stability Derivatives 22
4 Control Surface Deflections and Hinge Moments 22
5 Moments of Inertia 23
6 Modes at Level Flight 23
7 Static Stability Derivatives 27
8 Static Control Derivatives 27

Acronyms

GB	Golf Ball
FDR	Final Design Review
PB	Ping-Pong Ball
PDR	Preliminary Design Review
RC	Remote Control
TB	Tennis Ball
UTIAS	Univeristy of Toronto Institute for Aerospace Studies
AVL	Athena Vortex Lattice Solver
TE	Trailing Edge
LE	Leading Edge
AC	Aerodynamic Center
CG	Center of Gravity

1 Overview

The main decisions from our Preliminary Design Review (PDR) are briefly summarized in this section. Most of the decisions made in our PDR remain unchanged. The minor changes are stated and justified in this section.

1.1 Design Objectives

Our objectives have slightly changed from PDR after thorough analysis of the aircraft's performance. The major change is reflected in design objective 5, where after careful calculations, it was deemed infeasible to design for the take-off bonus (see Section 3.5 for more details). The design objectives and driving requirements for this aircraft are the following:

1. Design a stable conventional configuration aircraft with high-fidelity to its designed performance characteristics.
2. Complete the 3-lap course in 45 seconds or under[1].
3. Design the cargo to carry at least 20 golf balls[2].
4. Design an aircraft with a dry mass of 800 grams or lower[3]
5. Take off within 50 feet.
6. Design for dynamic stability during flight.
7. Achieve a flight score of 1000 points or greater.

1.2 Cargo Configuration

In our PDR, we evaluated the cost function in order to optimize our flight score. The main conclusion from that analysis showed that the cargo units score and payload factor should be maximized. The payload analysis concluded that using payload consisting only of golf balls would yield the highest payload mass for every target cargo unit score. This aircraft aims to carry a full load of 20 golf balls. The physical loading process is described in detail in Section 2.1.

1.3 Propeller Selection

The 9×6 propeller was selected for this aircraft, as it provides a good balance of both static thrust and pitch speed. Higher static thrust allows for a shorter take-off distance and higher take-off weight. A higher pitch speed will allow higher airspeeds. The propeller selection remains the same from PDR, but the geometry of our aircraft has changed (See Figure 14 in Section 3.1 for updated thrust curves).

[1] This will drive our design in determining wing dimensions and control surface sizing.

[2] A practical goal with high returns in score function. This is the largest direct factor in our flight score.

[3] This was determined by previous conventional Remote Control (RC) designs and allows the 1000+ points objective to be feasible. Minimizing mass also contributes to a higher thrust performance and a higher score in the scoring function.

1.4 Profile Selection

From our preliminary analysis, the SD7062 airfoil was selected for the main wing for this aircraft and remains unchanged. The tail, however, was chosen to be a balsa flat plate, rather than a foam NACA0012 as stated in PDR. This is mainly due to ease of construction as the balsa flat plate is lighter and structurally easier to attach to the rest of the plane. Trade-off and stall characteristics of these airfoils are detailed in PDR.

2 Detailed Design

This section presents a detailed overview of the airplane, with emphasis placed on the wing, fuselage, and the tail. The updated mass budget is presented as well. All these parts will be constructed out of balsa, unless otherwise stated. Each part will first be laser cut and then assembled using glue and other binding materials (e.g. hinge tape).

2.1 Fuselage

The fuselage is broken into two sections: main section and tail section. This was done to accommodate the laser cutter's size restriction of 12" $\times$ 24".

2.1.1 Main Fuselage

The main section of the fuselage lies directly underneath the wing and houses the primary cargo, which are the 20 golf balls. Since this fuselage will deal with the most strenuous loads (main wing lift and landing), it is reinforced with 6 bulkheads throughout its span (see figure 1). Each bulkhead has extensions on the sides and the bottom that fit into holes in the fuselage, thereby not only interlocking the two parts together, but also giving more surface area for the glue. Figure 2 shows the cross section of all the bulkheads in the main fuselage. Cutouts are made primarily for weight savings; bulkhead 1 has a solid piece in the middle for the engine mount. A 1/2" block of plywood will be glued to the fuselage under bulkhead 4 in order to provide extra support for landing loads. There is no structure on the top of the fuselage for weight savings purposes and to allow for hatches for loading the cargo and electronics. The rest of the fuselage pieces have cutouts for weight saving purposes. The fuselage side and bottom pieces, along with the bulkheads are 1/4" thick. The main fuselage has a constant cross section of $100mm \times 100mm$ and is $330mm$ long.

Figure 1: Fuselage Main Section

Figure 2: Main Section Bulkheads

(a) Bulkhead 1

(b) Bulkheads 2-6

2.1.2 Tail Fuselage

The tail section of the fuselage connects the main section to the tail of the airplane, and has a linearly decreasing cross section. This section also houses the secondary cargo, which are the 20 ping pong balls. Given that this section does not have to handle high loads, the cutouts made are quite large. Only two bulkheads are present in this section: the first one is there to keep the ping pong balls tightly packed, and the second is in the end to lock the fuselage's shape. Similar to the main section's bulkheads, both the tail section bulkheads have extensions on the two sides to interlock with the fuselage. There is also a cutout in the fuselage for the mount for the servos of the elevator and rudder, and to mount the horizontal tail. The tail section tapers from $100 \times 100mm$ cross section to $50 \times 50mm$, and is $610mm$ long.

Figure 3: Fuselage Tail Section

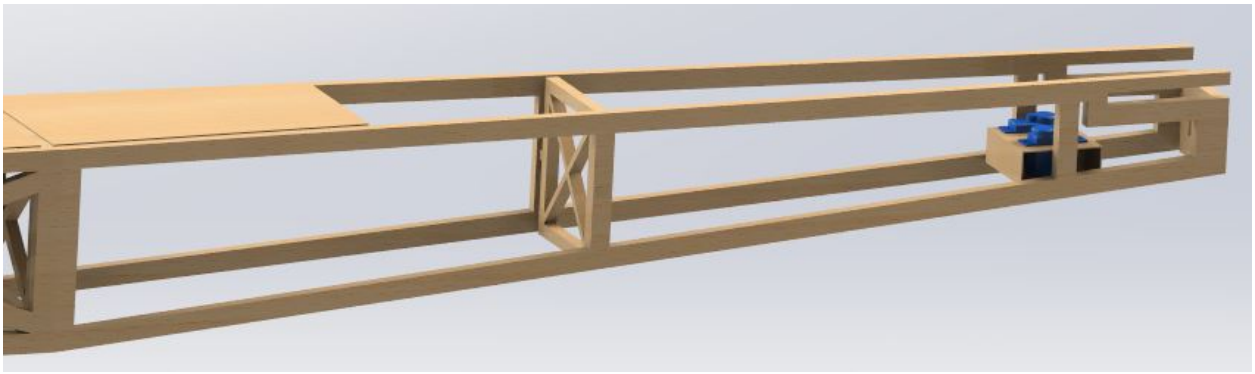

2.1.3 Cargo Placement

As mentioned before, the 20 golf balls will be placed in the main section and the 20 ping pong balls will be placed in the tail section of the fuselage. In the main section, the golf balls will be loaded via hatches 2, 3, and 4, while the ping pong balls will be loaded via hatch 5 (see figure 4). Electronics, such as the motor battery, will be placed between the first two bulkheads of the main section. The hatches will be attached to the fuselage using hinge tape.

Figure 4: Cargo Layout and Hatches

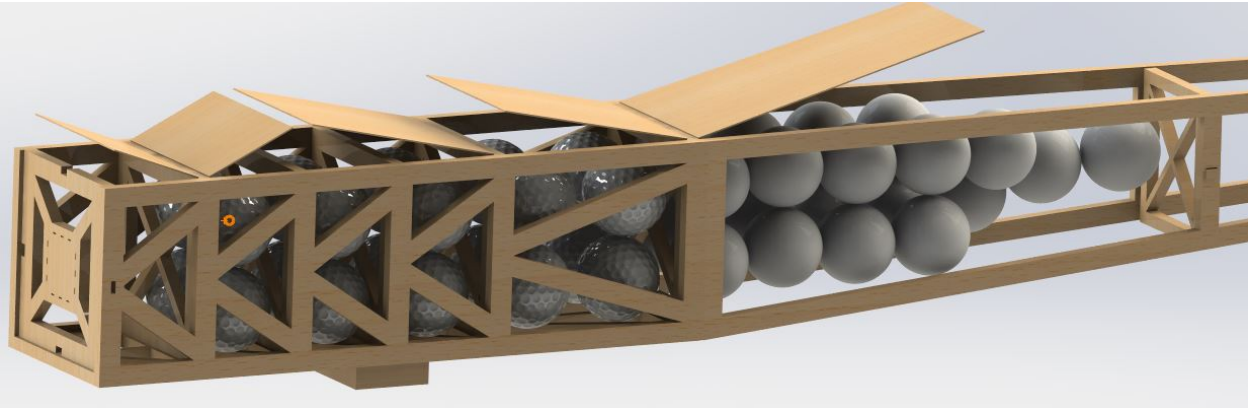

2.1.4 Engine Mount

The mount for the motor (figure 5) will be attached to bulkhead 1 via cutouts within the bulkhead. The cowling for the engine will be attached to the fuselage in a similar fashion.

Figure 5: Engine Attachment

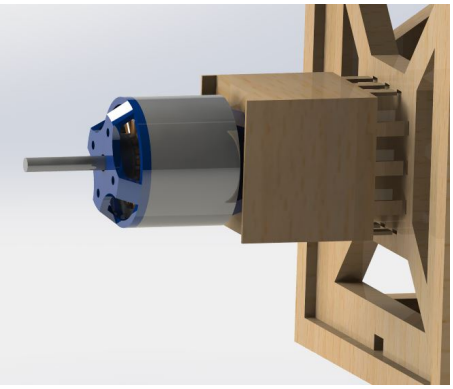

(a) Engine Mount

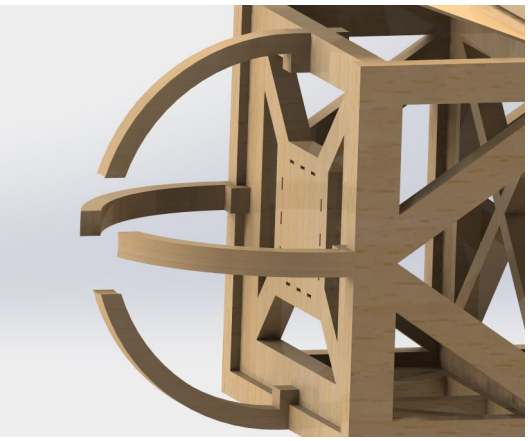

(b) Cowling

2.1.5 Wing Attachment

In order to load the cargo with ease, the wing will be constructed as a separated piece that will be attached to the fuselage using elastic bands. Figure 6 shows an example of the design. Such a configuration gives flexibility in the placement of the wing, which could be used to get a suitable static margin.

Figure 6: Example of Wing-Fuselage Attachment

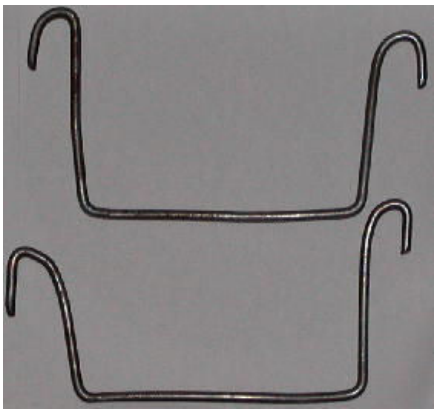

2.2 Wing

The wing will be constructed using a spar and rib method, primarily for weight savings purposes. The wing is split into three main sections: main spar, ribs, and rear spar.

2.2.1 Main Spar

The main spar is split into three sections in order to accommodate the laser cutter's restrictions. Each section will be 1/4" thick and will taper from 30 mm at the root to 27 mm at the tip. The middle section will be connected to the outer sections through glue and, in order to strengthen the mate, a piece of balsa wood will be glued to both sides of the main spar at that junction (see figure 7). Additionally, extra support is provided by gluing strips of balsa on the top and bottom of the main spar at the aforementioned locations. Cutouts have been made at intervals to lodge the ribs in place, and a cutout is made in the middle to attach the servo mount.

2.2.2 Ribs

There are 14 ribs along the span of the wing; this number was acquired from past designs and should provide reasonable tautness of the Monokote covering. A cross section of an aileron rib is presented in figure 8. All ribs have this cross section, with the exception of the cutout for the aileron. The first and last cutouts are made for the main spar and the rear spar. The cutout in the middle was made to save weight and to provide a passage for the push rods for the ailerons. The ailerons span across the last four ribs on each and are 25% of the chord of each of those ribs. The ailerons will be attached to the wing via hinge tape.

Figure 7: Main Spar

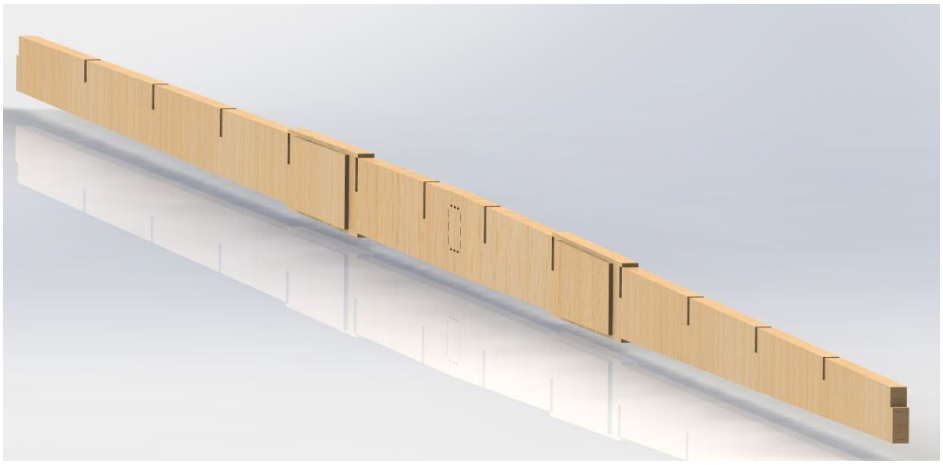

Figure 8: Rib Cross Section - Aileron

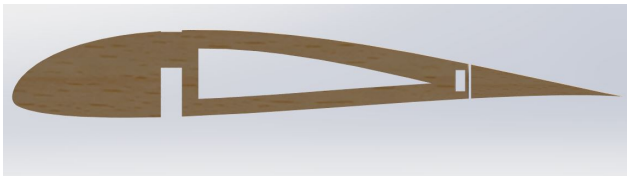

2.2.3 Rear Spar

The rear spar, similar to the main spar, runs through the ribs (figure 9). There are four pieces of the rear spar, with each side having two pieces (glued together).

Figure 9: Rear Spar

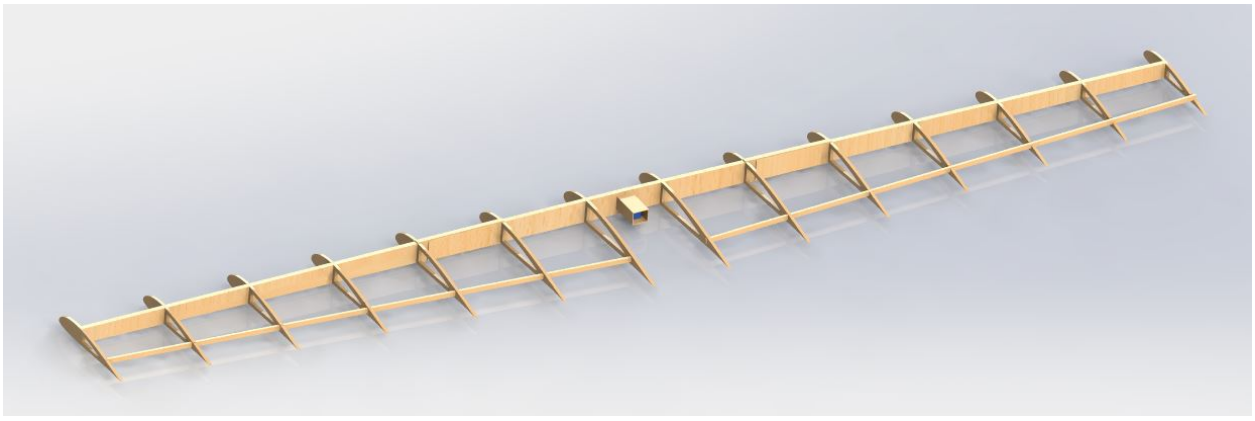

2.2.4 Servo Mount

The mount for the servo for the ailerons will be attached to the main spar via the cutouts made in the middle (figure 10).

Figure 10: Wing Servo Mount

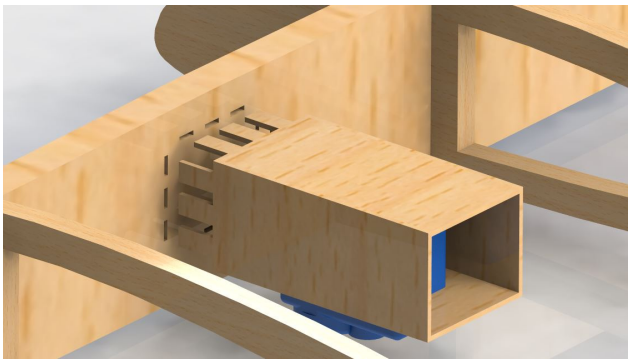

2.2.5 Sheeting

To provide surface for the Monokote covering to adhere to, a leading edge and trailing edge sheeting will be placed along the wing (figure 11). This sheeting will be made of 1 mm white foam, which is both light and easy to deform.

Figure 11: Wing Sheeting

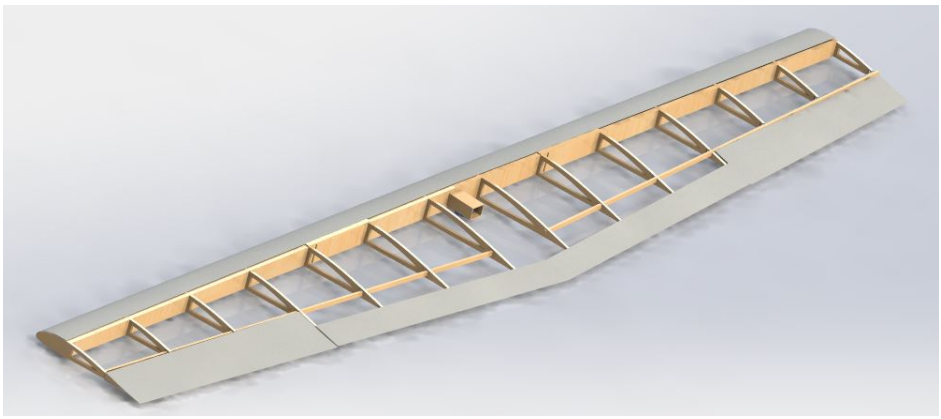

2.3 Tail

Both the horizontal and vertical tail are constructed as flat plates, which makes it easy to construct and mount them onto the fuselage (figure 12). Both flat plates are 1/4" thick and have cutouts for weight savings. The horizontal tail has slots in the beginning and middle that match the slots on the vertical tail and the side fuselage. This allows for the vertical tail to be mounted on top of the horizontal tail and glued securely before the latter is mounted onto the fuselage. Figure 13 shows how this mounting will be done. The elevator and rudder are both 40% of the root chord length, and span the entire length of each tail. Both control surfaces will be attached to the tail via hinge tape. As mentioned before, the mount for the two servos for the tail will be place inside the fuselage slightly aft of the tail. Cutouts in the side fuselage allow the mount to be secured in place.

Figure 12: Tail

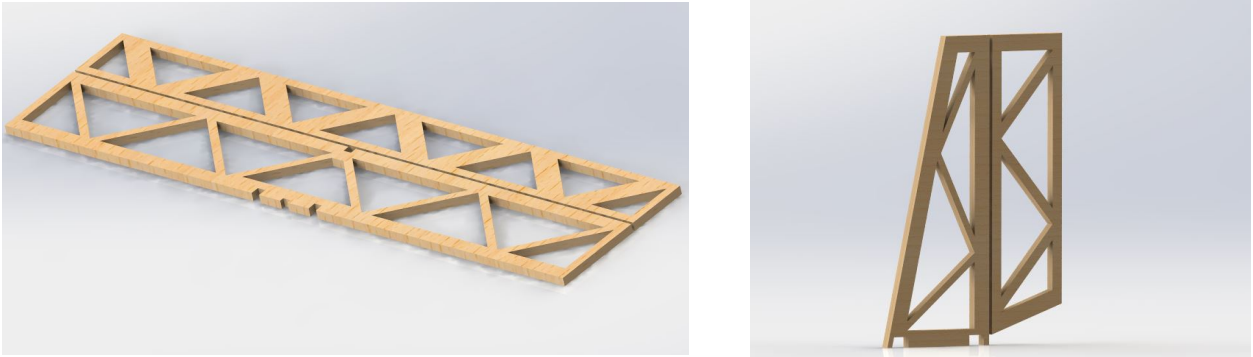

(a) Horizontal Tail

(b) Vertical Tail

Figure 13: Tail Fuselage Mounting

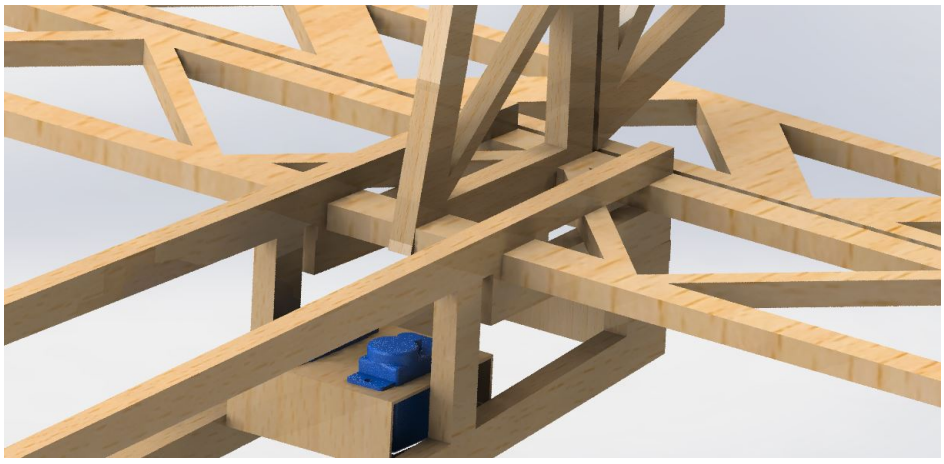

2.4 Mass Budget

By specifying the material densities in Solidworks, the following mass budget was acquired (table 1). A margin of 15% is used for the dry mass in order to account for material imperfections, construction errors, and the weights of the glue, Monokote, push rods, hinge tape, etc.

Table 1: Mass Budget

Part	Subcomponent	Mass (g)
Wing	Main Spar	41.58
	Ribs	20.18
	Rear Spar	4.52
	Sheeting	0.57
	Servo Mount	0.38
	Servo	7.94
	Total	75.17
Fuselage	Main - Sides	36.07
	Main - Bottom	14.07
	Main - Bulkheads	28.1
	Tail - Sides	29.82
	Tail - Bulkhead	3.4
	Landing Gear Attachment	7.1
	Total	118.56
Tail	Vertical Tail	9.01
	Horizontal Tail	27.3
	Servos	15.88
	Servo Mount	0.53
	Total	52.72
Propulsion	Motor	69.5
	Propeller	22.68
	Engine Cowling	1.55
	Engine Mount	0.59
	Total	94.32
Landing Gears	Main	185
	Tail	50
	Total	235
Avionics	**Total**	150
Dry Mass	No Margin	725.77
	15% Margin	**834.64**
Payload	Golf Balls	900
	Ping Pong Balls	54
	Total	954
Total Weight		**1788**

3 Performance Analysis

3.1 Level Flight

A drag model of the form in (3.1) was used for predicting max speed.

$$C_D = C_{D0} + KC_L^2 \tag{3.1}$$

The value of K was predicted using an inviscid model of the plane in Athena Vortex Lattice Solver (AVL). A contribution to C_{D0} from pressure drag on the wing and tail was also estimated from AVL. Viscous drag on the aerodynamic surfaces was computed using a flat plate model for skin friction given in (3.2).

$$C_{f,lam} = \frac{1.328}{\sqrt{Re_l}} \quad C_{f,turb} = \frac{0.074}{\sqrt{Re_l^{0.2}}} \tag{3.2}$$

The transition between laminar and turbulent flow occurs at $Re_l = 10^5$. While the position of x_{cr} varies with flight speed, it takes a minimum value of 44cm for a maximum possible flight speed of 17m/s. As this is substantially behind the Trailing Edge (TE), the main wing is considered to be laminar, while the body, horizontal tail, and vertical tail are considered to be turbulent. Contributions from each component are summarized in table 2.

Table 2: Drag Coefficient Breakdown

Element	C_{D0}
Wing	0.0053
Elevator	0.0093
Rudder	0.0029
Body	0.0401
Landing Gear	0.0040
Total	0.0616

Figure 14: Thrust Required and Thrust Available

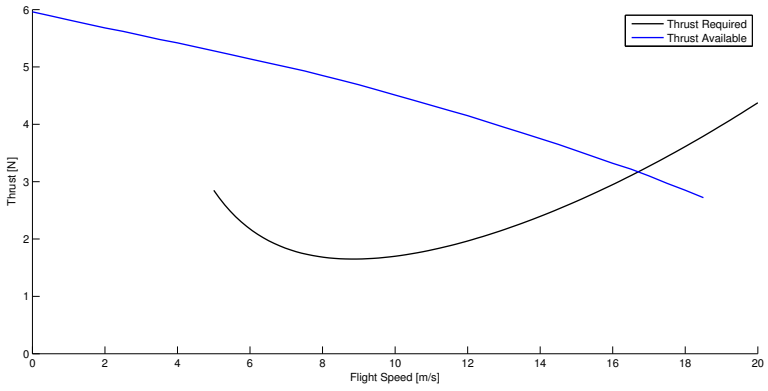

As both C_{D0} and K are dependant on flight speed–as C_L required for level flight decreases with increasing speed–several iterations were performed to estimate these

parameters. The maximum speed was calculated based on the thrust curve of a 9x6 propeller, and AVL simulations were re-run at this speed until this process converged on a maximum speed. The final results are shown in Figure 14, and the predicted maximum flight speed is 16.75m/s.

3.2 Turn

For this course, a level turn is not an accurate approximation of turning performance. The speed at which minimum turning time occurs is substantially less than the cruise speed, and the time required to decelerate/accelerate negates any performance increases from turning at this speed. Instead, a max load factor of 2.5 is assumed ($\phi = 66.5°$), based on a conservative $C_{L,max}$ of 1. Plots of turning radius and velocity over time are shown in Figure 15

Figure 15: Progession of a Turn

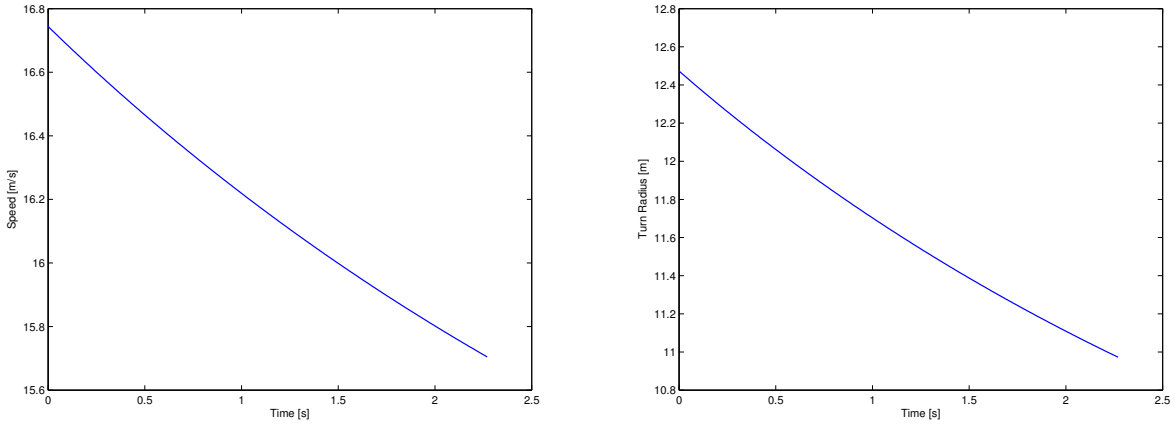

(a) Turn Speed

(b) Turn Radius

The turn takes approximately 2.25s to complete under these conditions, and has a radius between 11m and 12.5m which varies throughout the turn. A speed loss of 1m/s is incurred though the turn, which must be recovered over the straight leg of the course. This acceleration phase lasts the entire straight leg, and can be seen in Figure 16. This induces a time penatly on the straight leg, increasing the time for this section to 4.3s.

Figure 16: Acceleration After a Turn

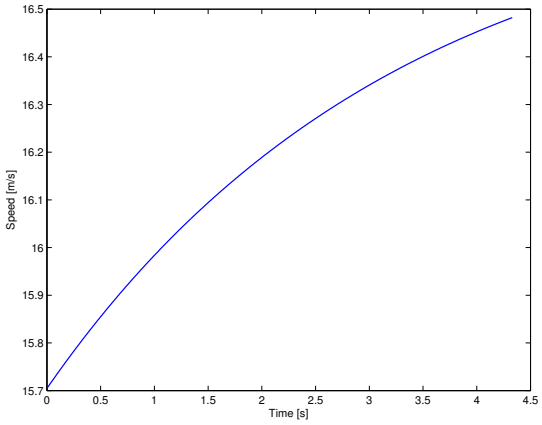

3.3 Structural Analysis

Structural analysis was conducted using finite element analysis for the main spar of the wing and the fuselage. The aircraft is mainly comprised of balsa and wood glue. All structural members are carefully designed to be able to piece together to minimize the stress on glue as shown in Section 2. The yield strength of balsa, on average, was found to be 20 MPa. The yield strength of balsa varies for different density and different grain direction. All loads have a large factor (3+) of safety in order to take into account the grain direction of balsa.

3.3.1 Main Spar

The main spar was loaded using outputs from AVL from aerodynamic analysis using finite element analysis. To be conservative, a higher estimate of the load distribution was calculated using the following equation.

The area of the elliptical loading was calculated using

$$\frac{\pi}{2}ab = 1.7gn$$

where $b = 1.5$ m, which is the span of the main spar, $1.7g$ is the static load of the aircraft without any external forces, and $n = 5$ is the load factor. The high load factor accounts for safety of factor, so there was no need to add in safety of factor. The maximum stress experienced was 19.5 MPa, which is fairly close the the yield strength of balsa. However, the high load factor accounts for this and we expect the main spar to experience less stress during flight and turns than this analysis. Deflection and strain analysis can be found in Appendix B.1.

Figure 17: Stress analysis on main spar loading

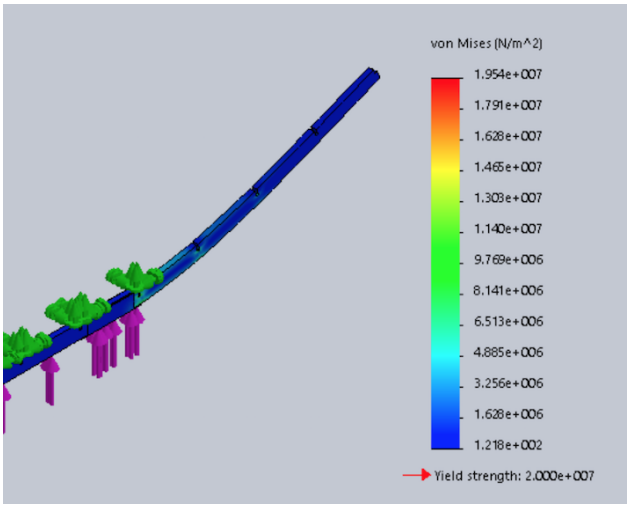

3.3.2 Tail

Finite element analysis was carried out to analyze the stresses at the tail. The tail was treated as a cantilever beam with a fixture at one end. A total of 10 N was applied to one end of the tail. As seen in Figure 18, the maximum experienced stress is 19 MPa, which is lower than the yield strength of balsa. At take-off and during flight, the maximum load on the tail was found to be 1.5 N at 15 degrees angle of attack from aerodynamic analysis. Thus, there is a multiple factor of 6, and the fuselage will withstand the loads experienced during flight and take-off.

Figure 18: Stress analysis on tail loading

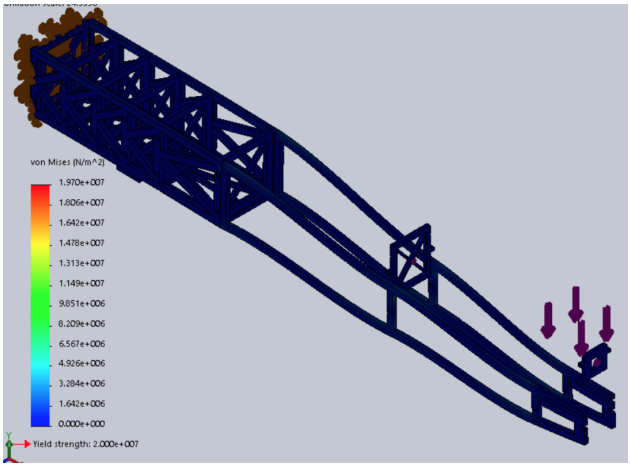

Finite element analysis was also used to analyze the stresses for both cargo loading and wing loading of the fuselage. The fuselage was fixed at one end and the cargo was loaded with 20 N of force, which is more than the weight of 20 golf balls with a safety factor of 2. The fuselage was also loaded with 45 N of upward force from the wing loading. 45 N was a reasonable estimate because the maximum load factor experienced during turns is 2.5 from aerodynamic analysis. Due to reliable trusses in the frame, the structure experience a maximum stress of 1.6 MPa, which is much less than balsa's yield strength (20 MPa). Hence, the fuselage will have no problem handling the stresses experienced during flight. Deflection and strain for both cases are listed in Appendix B.1.

Figure 19: Stress analysis on cargo loading

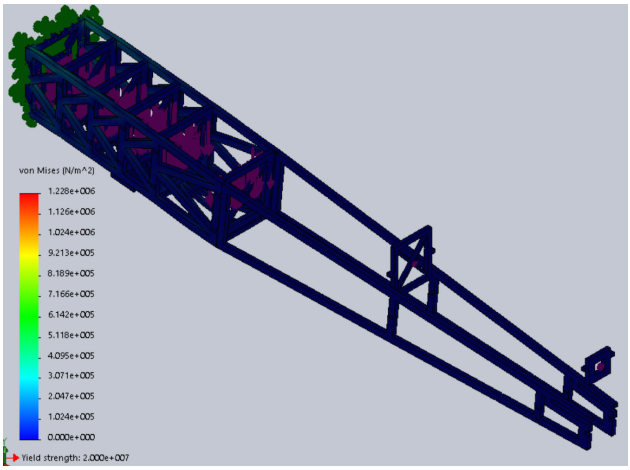

3.4 Stability

3.4.1 Static Stability

Static stability derivatives were evaluated in AVL. It was predicted for this plane that the Aerodynamic Center (AC) location was 12.5cm behind the wing Leading Edge (LE). The Center of Gravity (CG) location is discussed in Section **??**, and the mean aerodynamic chord is 18.5cm. This leads to a static margin of XX%, which is within the recommended value of 7%. Other stability derivatives were evaluated directly in AVL and the main quantities of importance are summarized in Table 3. See Appendix A for a complete table of stability derivatives.

Table 3: Static Stability Derivatives

Quantity	Value	Requirement
$C_{m\alpha}$	-0.7015	< 0
$C_{n\beta}$	0.0707	> 0
$C_{l\beta}$	-0.0244	< 0

3.4.2 Trim Deflections and Hinge Moments

The servo actuators used for this plane have a maximum rated torque of 18oz-in, or 0.128Nm. Using a factor of safety of 2, and the definition of the coefficient of hinge moment in (3.3), the maximum allowable coefficient of hinge moment is calculated as 6.58×10^{-3} (referenced to the main wing).

$$H_c = \frac{1}{2}\rho v^2 S\bar{c}C_{Hc} \tag{3.3}$$

Required hinge moments were calculated in AVL for a set of representative flight conditions: level cruise, maximum angle of attack, minimum angle of attack, and turn. Results for the required deflection and coefficient of hing moment are shown in Table 4.

Table 4: Control Surface Deflections and Hinge Moments

	Elevator		Ailerons		Rudder	
Condition	$\delta_c[^\circ]$	$C_H \times 10^4$	$\delta_c[^\circ]$	$C_H \times 10^4$	$\delta_c[^\circ]$	$C_H \times 10^4$
Cruise	0.57	1.01	0.00	0.00	0.00	0.00
$\alpha = 15^\circ$	-7.19	4.58	0.00	0.00	0.00	0.00
$\alpha = -5^\circ$	1.56	5.49	0.00	0.00	0.00	0.00
$\phi = 66.5^\circ$	4.89	3.66	0.52	3.62	1.06	0.24

It is evident from this analysis that the expected maneuvers of the plane are well within the control actuators' physical limits. It is also seen that the maximum required deflections are small ($\delta_c < 5^\circ$ for standard maneuvers and $\delta_c < 7.5^\circ$ for worst case scenario) indicating that the control surfaces have been sized appropriately to avoid flow separation.

3.4.3 Dynamic Stability

Dynamic stability was analyzed in AVL. Moments of inertia were extracted from the CAD model, and are summarized in Table reftab:inertia, where m, n, and l have been substituted for the standard xyz coordinate system.

Table 5: Moments of Inertia

Axis	Inertia $[kgcm^2]$
I_{ll}	125.5
I_{mm}	353.6
I_{nn}	237.7

Analysis resulted in 8 eigenvalues, with 3 conjugate pairs. These values corresponded to the Dutch Roll (roll-yaw coupling), Phugoid, Short Period, Spiral, and Roll Damping modes. Frequency and damping properties were computed for each mode, and results are summarized in Table 6.

Table 6: Modes at Level Flight

Name	Eigenvalue	$t_{1/2}[s]$	ζ	$\omega_n[rad/s]$
Roll	-132.5	0.005	-	-
Dutch Roll	$-5.391 \pm 13.89j$	0.129	0.362	14.90
Short	$-18.92 \pm 7.582j$	0.037	0.928	20.38
Spiral	0.081	8.601	-	-
Phugoid	$-0.107 \pm 0.518j$	6.482	0.202	0.259

The first 3 modes are strongly damped, and will not provide any problems in level flight. The phugoid mode, while stable, is much more lightly damped, and may lead to some loss of performance if strongly perturbed. The spiral mode is not stable for this plane, however unstable modes with a doubling time of greater than 4s can be handled by pilot correction. Since this constraint is met for the spiral mode, stability issues are not expected for level flight.

3.5 Take-off

Takeoff analysis was performed by numerically integrating the thrust and drag forces. The coefficient of lift was taken as $C_{L,max} = 1.1$ and the ground effect on the drag coefficient was modeled by Equation (3.4).

$$C_{D_G} = C_{D_0} + \phi K C_L^2 \quad \phi = \frac{(16h/b)^2}{(16h/b)^2+1} \tag{3.4}$$

The net force on the plane during takeoff is then modeled by (3.5), where available thrust varies with speed as discussed in Section 3.1, and $\mu = 0.04$ for wood was assumed.

$$F_{net} = T(v) - qC_{D_G} - \mu\left(1 - \frac{qC_L}{W}\right) \tag{3.5}$$

The net force was integrated numerically, starting from zero initial position and an initial velocity equal to the headwind, until the takeoff velocity was reached. Takeoff

Figure 20: Takeoff Distance vs Headwind

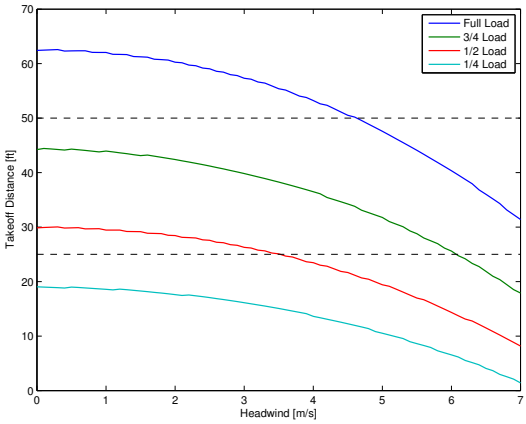

distance for various headwinds and loading configurations is shown in Figure 20. For the full loading case, a headwind of 4.5m/s is required to takeoff within 50ft. All other loading cases can takeoff within the allotted runway space without headwind, and may acquire a takeoff bonus depending on the strength of the wind.

4 Flight Score Prediction

The flight score for any given run can be evaluated as per Equation 4.1

$$FS = CU \times f(t) \times PF \times TB \times CB + PPB \tag{4.1}$$

Where CU is the number of cargo units carried, PF is fraction of total mass made up of cargo, TB is a takeoff bonus of 1.2 if takeoff is achieved within 25 feet, CB is a fixed configuration bonus of 1, and $f(t)$ is given be (4.2).

$$f(t) = e^{1.5\left(1-\frac{t}{65}\right)} \tag{4.2}$$

As discussed in Section 3.2, the length of a turn is 2.3s, however the loss of speed is not completely made up during the straight leg of the course, causing subsequent turns to take different lengths of time. The time taken on the course was therefore calculated as one straight leg at max speed, followed by 5 turn and acceleration phases. This analysis results in a total flight time of 37.1s, or a flight time multiplier of 1.9.

Figure 21: Flight Score vs Headwind

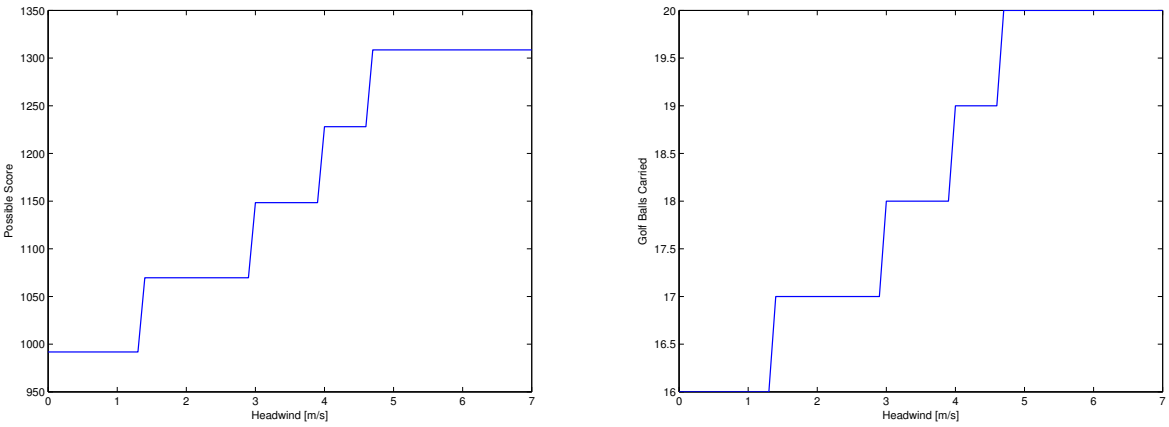

(a) Ttotal Score

(b) Golf Balls Carried

Cargo units carried, payload fraction, and takeoff bonus are all closely linked. Increasing the number of golf balls carried increase cargo unit score and payload fraction, but require longer takeoff distances. Applying the analysis of Section 3.5 to varying numbers of golf balls from 0 to 20, the maximum possible score may be found as a function of headwind, which is the only variable that cannot be controlled for. As can be seen in Figure 21, the possible scores of this plane range between 990 and 1310 points.

5 Future Work

Future work consists mainly of construction and testing of the craft. The detailed CAD models presented here will provide all of the necessary shapes to be cut out by the laser cutter, which will be assembled, fit with electronics, and then covered in Monocote to provide a smooth finish. Leading and trailing edge padding will be constructed with the foam cutter. This work will need to be completed by April 3rd in order to meet the zipline test deadline. The remaining time before flyoff will be dedicated to testing and making minor physical adjustments to improve performance and ensure stability in flight.

A Static Derivatives

This appendix contains the complete table of static stability derivatives and control derivatives.

Table 7: Static Stability Derivatives

Coefficient	α	β	Roll Rate $\dot{p}$	Pitch Rate $\dot{q}$	Yaw Rate $\dot{r}$
C_L	5.2364	0.0000	0.0001	8.1618	0.0000
C_Y	0.0000	-0.2155	0.0354	0.0000	0.1511
C_l	0.0000	-0.0244	-0.5148	0.0000	0.0983
C_m	-0.7015	0.0000	0.0000	-20.5248	0.0000
C_n	0.0000	0.0707	-0.0213	0.0000	-0.0718

Table 8: Static Control Derivatives

Coefficient	Aileron δ_a	Elevator δ_e	Rudder δ_r
C_L	-0.0000	0.0118	0.0000
C_Y	-0.0003	0.0000	-0.0024
C_l	0.0094	0.0000	-0.0002
C_m	0.0000	-0.0412	0.0000
C_n	0.0005	0.0000	0.0011
C_D	0.0000	0.0009	0.0000
e	0.0000	-0.1308	0.0000

B Calculations

B.1 Structural Analysis

Figure 22: Finite Element Analysis on Fuselage

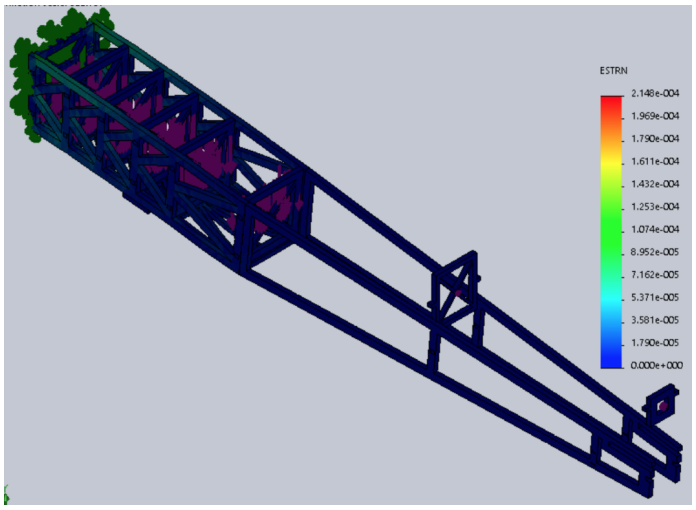

(a) Strain of Cargo loading

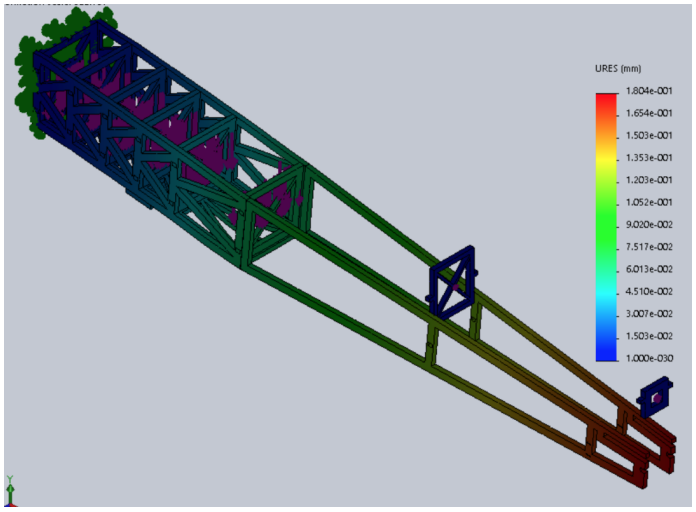

(b) Deflection of cargo loading

Figure 23: Finite element analysis of tail

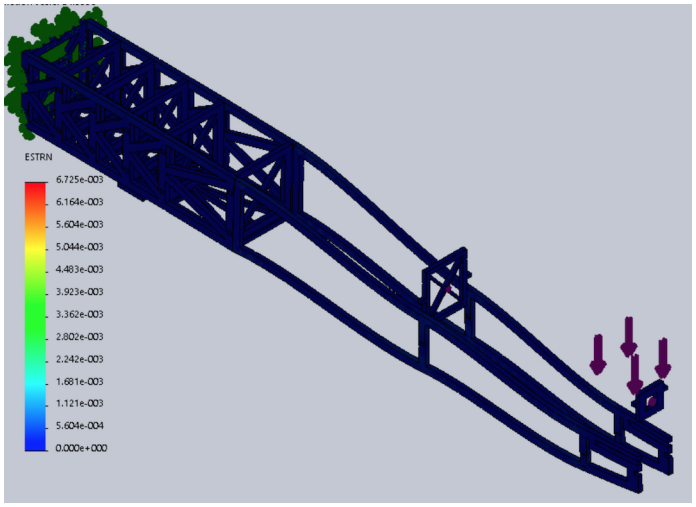

(a) Strain of tail loading

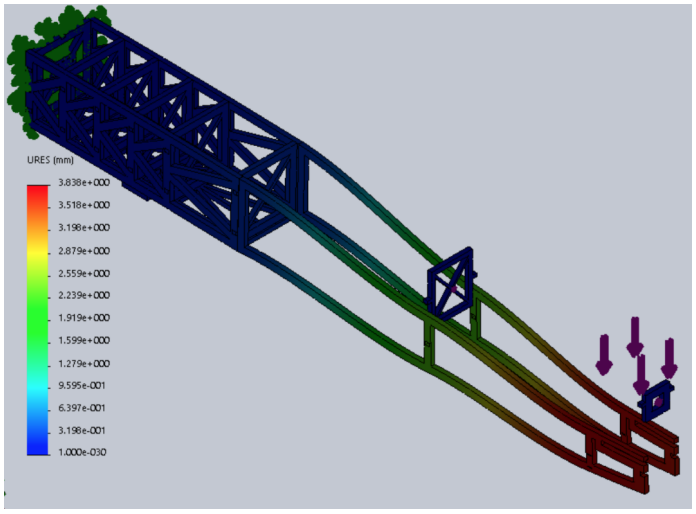

(b) Deflection of tail loading

Figure 24: Finite element analysis of main spar

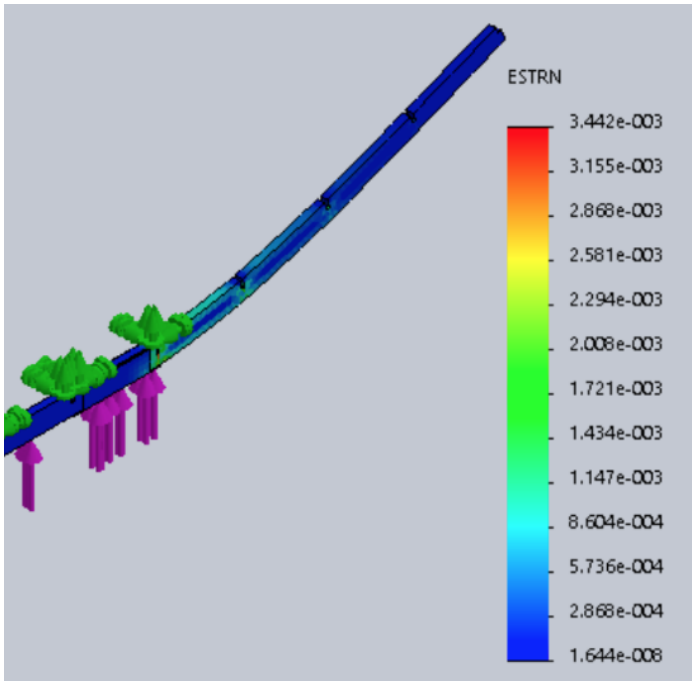

(a) Strain of Main Spar

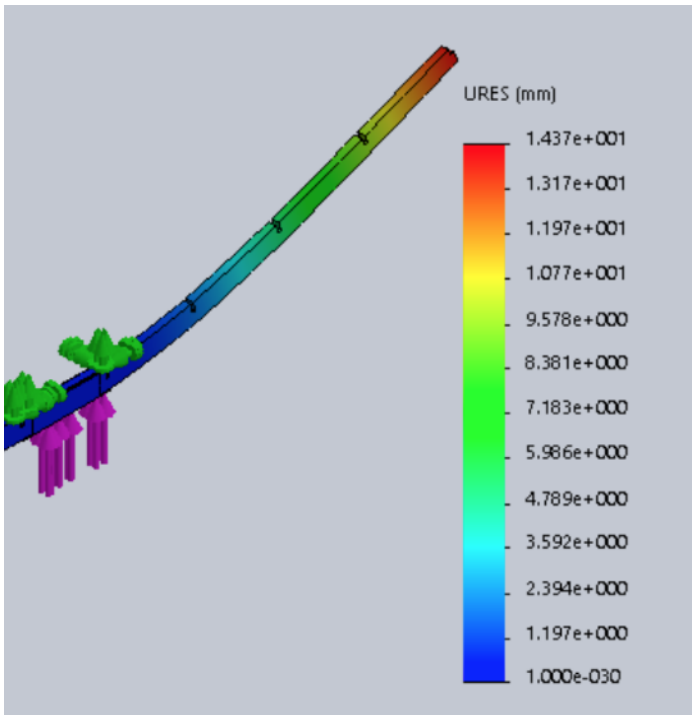

(b) Deflection of Main Spar